Minireview

Shape-specific polymeric nanomedicine: emerging opportunities and challenges

Li Tao[1], Walter Hu[1], Yaling Liu[2], Gang Huang[3], Baran D Sumer[4] and Jinming Gao[3]

[1]Erik Johnsson School of Engineering & Computer Science, University of Texas at Dallas, Richardson, TX 75080; [2]Department of Mechanical Engineering and Mechanics, Lehigh University, 19 Memorial Drive West, Bethlehem, PA 18015; [3]Department of Pharmacology, Harold C Simmons Comprehensive Cancer Center; [4]Department of Otolaryngology, University of Texas Southwestern Medical Center, Dallas, TX 75390, USA

Corresponding author: Dr Jinming Gao, Department of Pharmacology, Harold C Simmons Comprehensive Cancer Center, University of Texas Southwestern Medical Center, 5323 Harry Hines Blvd, Dallas, TX 75390, USA. Email: jinming.gao@utsouthwestern.edu

Abstract

Size and shape are fundamental properties of micro/nanoparticles that are critically important for nanomedicine applications. Extensive studies have revealed the effect of particle size on spherical particles with respect to circulation, extravasation and distribution *in vivo*. In contrast, the importance of particle shape has only recently begun to emerge. For example, cylindrically-shaped filomicelles (diameter 22–60 nm, length 8–18 μm) have shown persistent blood circulation for up to one week after intravenous injection, much longer than their spherical counterparts. Disc-shaped nanoparticles have demonstrated higher *in vivo* targeting specificity to endothelial cells expressing intercellular adhesion molecule receptors in mice than spherical particles of similar size. In this Minireview, we will discuss the recent advances in the fabrication of shape-specific nanoparticles and their unique biological and pharmacological properties. Computational models are presented to provide mechanistic understanding of the shape effects on cell targeting under flow conditions. Shape-specific nanoparticles have the potential to significantly improve the performance of nanomedicine in diagnostic imaging and targeted drug delivery applications.

Keywords: shape-specific nanomedicine, non-spherical nanoparticles, top-down engineering method, drug delivery, intravascular dynamics, cell targeting

Experimental Biology and Medicine 2011; **236**: 20–29. DOI: 10.1258/ebm.2010.010243

Introduction

Nanomedicine is a rapidly evolving discipline that applies the advances in nanotechnology for diagnosis and treatment of diseases.[1–3] Examples include the development of targeted nanoparticles capable of delivering therapeutic and diagnostic agents to specific biological targets.[3–11] In a nanoparticle-based platform, therapeutic drugs or imaging agents are encapsulated in polymeric carriers, providing multiple advantages over conventional small molecular formulations, such as cell targeting, reduction of clearance and systemic toxicity, the ability to deliver large payloads of hydrophobic drugs and the potential for incorporating multiple payloads in a single carrier for multifunctional applications.[4,5,10–12]

Over the past few decades, various nanoplatforms, including liposomes,[13,14] polymeric micelles,[15,16] quantum dots,[17,18] Au/Si/polymer shells[19,20] and dendrimers[21,22] have been established with distinctive chemical compositions and biological properties. Most current nanoparticulate systems are spherical in shape, and extensive work has been dedicated to studying their biological behaviors *in vitro* and *in vivo*. Similar to size, shape is a fundamental property of micro/nanoparticles that is critically important for their intended biological functions.[23] Unlike size, the biological effects of particle shape are less well understood. Recent data have shown that particle shape may have a profound effect on their biological properties. For example, cylindrically shaped filomicelles can effectively evade non-specific uptake by the reticuloendothelial system, allowing persistent circulation for up to one week after intravenous injection.[24] Theoretical modeling work has shown that non-spherical particles can significantly increase particle adhesion to cellular receptors under flow conditions compared with spherical particles. Experimentally, Muzykantov and co-workers[25] showed that disk-shaped nanoparticles ($0.1 \times 1 \times 3$ μm) increased (>20 times increase in immunospecificity index) particle targeting

to intercellular adhesion molecule 1-expressed pulmonary endothelium over spherical particles of similar size. Other non-spherical nanoparticles (e.g. carbon nanotubes,[26] worm-shaped iron oxide nanoparticles[27,28]) have also demonstrated considerably increased accumulation and retention in tumor tissues *in vivo*. These data, as well as a wide array of naturally occurring shape-specific nanoparticulates shown in Figure 1, are beginning to highlight the importance of controlling particle shape for nanomedicine applications.

Despite these early studies, there still is a lack of systematic and fundamental understanding of how shape affects the *in vivo* behavior of nanoscale constructs. One contributing factor is that conventional fabrication methods are limited in their ability to control the shape and size of nanoparticles simultaneously. This limitation hinders direct investigation of the effects of shape independent of size or other factors. There is also a lack of integration between computational modeling and experimental validation, an important requirement for understanding the effects of shape at nanoscale in the biological systems. This paper will review the current methods for producing shape-specific nanoparticles and highlight the preliminary findings with respect to their biological and pharmacologicol properties. Also, recent computational modeling strategies for assessing the intravascular dynamics and cellular uptake of particles relative to their shape *in vivo* will be discussed.

Fabrication of shape-specific nanoparticles

Both bottom-up chemistry and top-down engineering methods have the capability to produce polymeric nanostructures. Most polymeric nanoparticles currently used for biomedical applications are produced using bottom-up methods.[29,30] These methods can produce nanoparticles with a spherical shape and a wide variety of sizes driven by favorable thermodynamics leading to the self-assembly of the nanoparticles.[31] Although non-spherical shapes are possible using diblock co-polymers, size and shape are difficult to control independently using bottom-up methods. Several bottom-up techniques have been developed to fabricate non-spherical particles.[27,32,33,47] As shown in Table 1, Geng *et al.*[24] employed a self-assembly method to produce polyethylene glycol (PEG)-based filomicelles loaded with the antineoplastic agent paclitaxel. Park *et al.*[27] synthesized magnetic iron oxide worm-shaped clusters in the presence of higher molecular weight dextran. Yang *et al.*[47] reported the formation of high aspect-ratio ellipsoidal polymeric nanoparticles using a miniemulsion technique. Although all show exciting results with interesting science, most of these methods still lack precise and uniform control over shape and size independently. Currently, the bottom-up methods will be limited in the production of non-spherical nanoparticles, with systematic change of one dimension at a time to test shape-specific hypotheses in biology.

In contrast, polymers can be precisely patterned and used as resistors for microelectronic applications, with good control over their final shape using electron, ion or photon beam lithographic techniques. The costliness of these techniques has led to the development of low-cost top-down techniques, such as nanoimprint lithography,[48,49] soft lithography[50] and others.[51–55] Table 1 summarizes some of the processes used to produce non-spherical polymeric particles, including particle replication in non-wetting templates (PRINT®),[56] elastic stretching of spherical particles,[40] step-flash imprint lithography (S-FIL)[43] and template-induced printing (TIP).[44–46] These techniques have obtained promising results in manufacturing non-spherical platforms for nanomedicine applications.

Particle replication in non-wetting template

The PRINT® process,[56] a derivative form of the soft lithography method, can be used to create isolated nanoparticles of various shapes using perfluoropolyethers (PFPE) as a template. The mechanism to fabricate polymeric structures is as follows: a template containing cavities with a predesigned shape and size are pressed into a thin film of polymer or solution. The polymer is filled into the cavities and then solidified either by cross-linking or by the evaporation of solvent. This procedure usually leads to a residual layer (called 'scum' or 'residue') that interconnects the patterned particles on the substrate,[57,58] preventing the dispersion of particles. The key success of PRINT® is the residue-free fabrication with PFPE as a template. The PFPE surface allowed for selective filling of polymers into cavities without wetting the surrounding area, allowing the formation of distinct particulates[56] that can then be easily harvested.[59] Together with other advantages from PFPE,[60] PRINT® holds the promise of generating shape-specific nanoparticles in high throughput.

As shown in Table 1, PRINT® has great flexibility with respect to the matrix materials that can be utilized to

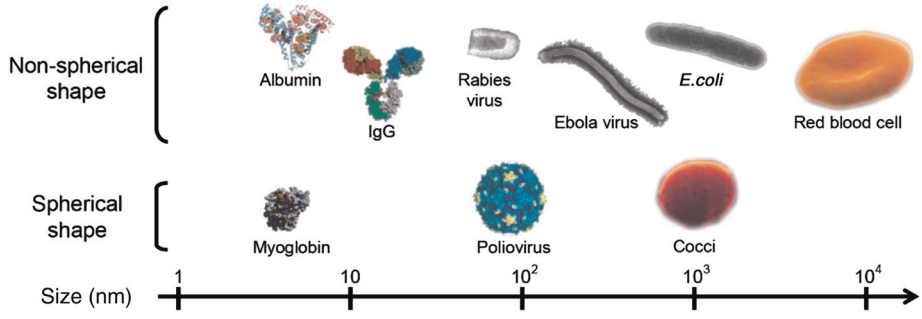

Figure 1 Size and shape comparison of various naturally occurring nanoparticulate objects (A color version of this figure is available in the online journal)

Table 1 Various fabrication techniques on shape-specific nanoparticles

Fabrication techniques		Shapes	Smallest dimension	Matrix materials	Incorporated functional agents	References
Top-down approach	PRINT®	Cube, rod, circular disc, cone, hex-nut	100 nm	PEGDA, PLA, PPy, triacrylate, natural proteins	Cy3 dye, doxorubicin, Fe_2O_3, Gd-DOTA, protein	34–39
	Stretching spherical particles	Elliptical disc, oblate or prolate ellipsoid, worm, UFO	200 nm	Polystyrene, PLGA	FTIC-labeled bovine serum albumin	40–42
	Step-flash imprint lithography	Square, triangle, pentagon	50 nm	PEGD(M)A, PEGDA-GFLGK-DA	Streptavidin-Cy5 fluorescent dye, plasmid DNA	43
	Template-induced printing (TIP)	Circular disc, bullet, rod, long worm	80 nm	SU-8, PEGDA, PEG-b-PLA	BODIPY dye, SPIO (Fe_3O_4)	44–46
Bottom-up approach	Self-assembly	Long worm	22–60 nm	OE, OCL	Paclitaxel	24
		Worm	5 nm (Fe_2O_3 diameter)	Fe_2O_3	N/A	27
	Emulsion	Ellipsoid	28 nm	F8BT, PFO	N/A	47

PEGDA, polyethylene glycol diacrylate; PLA, poly(D,L-lactic acid); PPy, poly(pyrrole); PLGA, poly(D,L-lactic acid-co-glycolic acid); PEGDMA, polyethylene glycol dimethacrylate; PEGDA-GFLGK-DA, poly(ethylethylene glycol diacrylate-co-acrylated Gly-Phe-Leu-Gly-Lys); PEG-b-PLA, poly(ethylene glycol)-co-poly(D,L-lactic acid); OE, PEG-polyethylene; OCL, PEG-poly(ε-caprolactone); F8BT, poly(9,9-dioctylfluorene-cobenzothiadiazole); PFO, poly(9,9-dioctylfluorene); Gd-DOTA, Gd-1,4,7,10-tetraazacyclododecane-1,4,7,10-tetraacetic acid; SPIO, superparamagnetic iron oxide; UFO, unidentified flying object

create a variety of shapes such as cubes,[36,37,61] circular discs,[38,62] rods[38,63] and cones[38] as well as others.[61] Successful incorporation of anticancer drugs[37] or imaging agents[35,62] has also been demonstrated. A few representative examples include $\Phi 150 \times 450$ nm PEG hydrogel rod containing antisense oligonucleotide (Figure 2a1), 3 μm hallow hex-nuts (Figure 2a2) and $\Phi 200 \times 200$ nm PEG rods containing 15% iron oxide (Figure 2a3 and a4) as non-spherical agents for magnetic resonance imaging.

Stretching of spherical particles

The first demonstration of stretching spherical particles into non-spherical shapes was reported by Ho *et al.*[42] Polystyrene spheres were embedded in a polymer film to create ellipsoidal particles by stretching the film. Mitragotri and co-workers[40] modified this technique to generate polystyrene particles with over 20 different shapes as partially listed in Table 1. A large variety of shapes can be achieved using this technique by adjusting parameters such as the aspect-ratio of stretching, the thickness of the film or method used to liquefy the polystyrene particles.[41] The smallest size reported by this method is a few hundred nanometers (Figure 2b1) in the smallest dimension with a high aspect-ratio of ~20. Typical sizes for these particles range from 1 to 10 μm (Figure 2b2) in each dimension. The throughput has been reported at 10^8–10^{12} particles per stretching apparatus depending on the intended final size of the particles.[40,41] One limitation of this technique is the quality of the starting spheres, which directly impact the uniformity of shape and size for the final particles.

Step-flash imprint lithography

S-FIL[49] is a commercially available (Molecular Imprint®) nanoimprint process that employs a quartz template and utilizes a mechanism similar to soft lithography. Cross-linkable polymer fills into the cavities of the template and is exposed to ultraviolet (UV) light for cross-linking. Roy *et al.*[43] applied S-FIL to PEG-based polymers with an underlying water soluble polyvinyl alcohol (PVA) layer used for releasing the particles. Nanoparticles cubes, triangles (Figure 2c1) and pentagons (Figure 2c2) with incorporated biofunctional agents have been fabricated with sizes $\leq$50 nm (Table 1). They have also demonstrated enzyme-triggered release of plasmid DNA from the nanoparticles *in vitro*. Although the method offers great control over shape and size simultaneously, the residue layer remains a major limitation of S-FIL. Reactive ion etching employed to remove the residue not only exposes biomaterials to a harsh environment that can lead to degradation of the polymers and entrapped biological agents but also increases the time and cost of this process.

Template-induced printing

WH's and JG's labs have established several top-down methods using templates to generate non-spherical polymeric particles with a variety of aspect-ratios (γ) and local shapes (Table 1). Low aspect-ratio objects such as discs ($\gamma < 0.1$) with the smallest dimension of a few hundred nanometers in height were fabricated using the photolithography method on a bi-layer polymer film. The bi-layer structure is a stack of functional polymer such as epoxy-based SU-8 (Microchem®) or polyethylene glycol diacrylate (PEGDA) on top of a sacrificial layer such as polymethylmethacrylate or PVA. Functional polymer film was selectively exposed to UV light through a photomask to cross-link only the exposed area. A proper solvent eventually dissolves the non-exposed polymers. This process has been used to fabricate 2–3 μm PEG discs (Figure 2d1) in a variety of heights ranging from 100, 200 to 500 nm

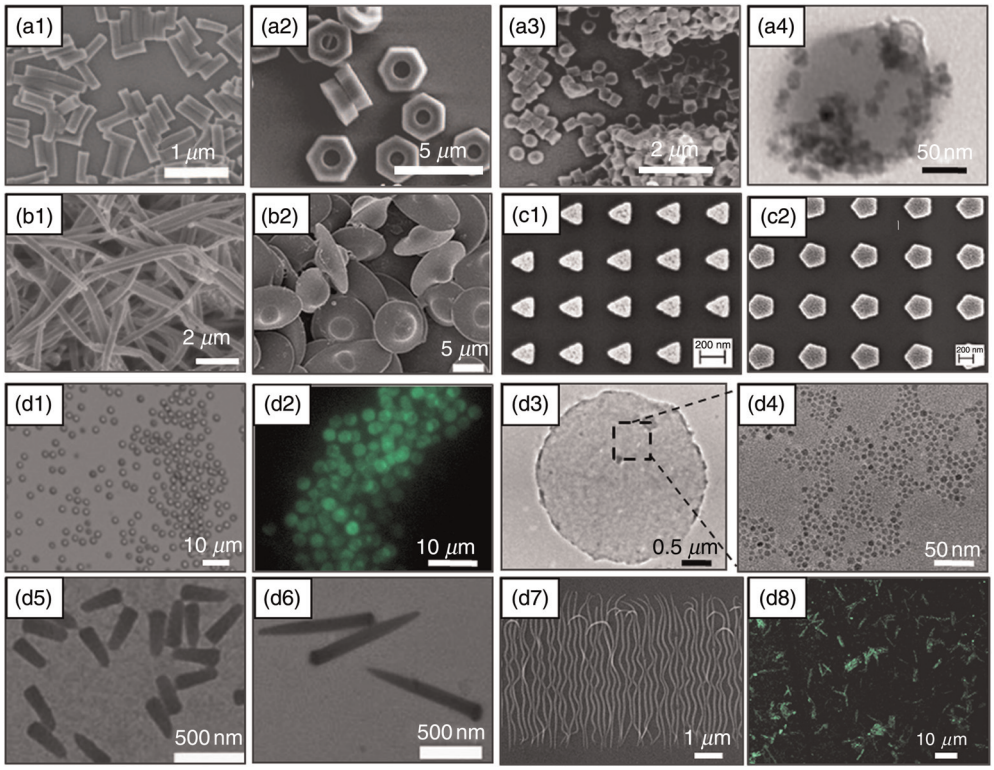

Figure 2 Top-down fabrication of shape-specific nanoparticles. (a) Particles by PRINT® method: (a1) PEG cylindrical rods with 150 nm diameter and 450 nm length; (a2) 3 μm PEG 'hex-nuts'; (a3) cylindrical particles of 200 nm in diameter and 200 nm in height; (a4) 15 wt% PEG-silane-coated iron oxide (Fe_2O_3) nanocrystals. (b) Stretching polystyrene particles: (b1) worms of 220 nm in diameter with aspect-ratio of ~20; (b2) UFOs. (c) S-FIL PEGDA particles: (c1) 200 nm triangles; (c2); 400 nm pentagons. (d) Template induced printing of nanoparticles: (d1) 2.5 μm PEGDA discs with 100 nm thickness and (d2) fluorescent images after releasing into aqueous solution; (d3 and d4) 2 μm SU-8 discs loaded with 10wt% superparamagnetic iron oxide; (d5 and d6) SU-8 bullets of 80 nm in diameter and 300 and 900 nm in length, respectively; (d7) BODIPY-containing SU-8 worms with 80 nm diameter and 6 μm length (aspect-ratio 75); and (d8) fluorescent image of d7 in aqueous solution. Reprinted with permissions from corresponding references. PRINT, particle replication in non-wetting template; PEGA, polyethylene glycol; S-FIL PEGDA, step-flash imprint lithography polyethylene glycol diacrylatel; UFO, unidentified flying object (A color version of this figure is available in the online journal)

with water as the solvent for releasing and harvesting the particles. Fluorescent images of these PEG discs after collection verified good preservation of incorporated BODIPY fluorophores (Figure 2d2). In hydrophobic SU-8 discs (Figure 2d3), 0.06 wt% BODIPY dye (low density was used to avoid auto-quenching) and 10 wt% superparamagnetic iron oxide (SPIO) were loaded together. Transmission electron microscopy bright field images (Figure 2d4) of SPIO crystals inside hydrophobic discs show relatively uniform distribution without clustering. This fluorescent-magnetic disc is a good example of a multifunctional platform with independent control over shape, size and chemical composition. Current yield for this process is 10^8–10^9 particles per run on a 4″ Si wafer depending on the size of the particles.

Nanoparticles with $\gamma > 1$, such as rods (Figure 2d5) or bullets (Figure 2d6), have also been fabricated using a bi-layer nanoimprint process.[44] With careful control over the thickness of both layers and following the geometry of cavities in the template, functional polymer is slowly depleted during the filling of the template cavities, allowing the sacrificial layer to partially fill into the cavities. As a result, the residue layer only occurs in the sacrificial polymer and is separated from the nanopillars in the functional polymer. This engineering control allows the release of imprinted nanopillars without the need for plasma etching to remove the residue. Another feature of this process is the high-density template duplicated from the anodic alumina membrane, yielding 10^{10} particles per cm^2. Recently, we adapted this bi-layer nanoimprint technique to generate worm-shaped nanoparticles with an ultra-high aspect-ratio.[46] Fluorescent nano-worms with a diameter of 80 nm and length of 6 μm ($\gamma \sim 75$) were fabricated and collected in water (Figure 2d7 and d8). These data demonstrate the capability of our method to produce ultra-long worm-shaped particles, which have been most often reported for nanomedical applications.[24,41,61] Our lithographically defined worms are well controlled in shape, size and uniformity compared with filamentous particles made by conventional self-assembly methods.[24,27,47] The capability to produce mono-dispersed particles is essential to extract the independent effect of shape, which is indistinguishable from the interplay of size and shape for conventional particles.

Another method, combining top-down and bottom-up strategies, was established from surface energy induced patterning (SEIP)[45] to generate shape-specific particles. It employs a template with discrete and different surface energies. The chemically heterogeneous surface of the template can induce self-organization of the spin-on polymer thin film by thermal annealing at a temperature above its glass

transition temperature (T_g). Due to the lack of residue during fabrication, SEIP particles can be harvested from the template surface to aqueous solution using a bath sonication process. SEIP is applicable to many materials, such as SU-8 and PEG-b-PLA polymers.[45]

In summary, these top-down methods (PRINT®, stretching of spheres, S-FIL and TIP) share several common features. All these methods demonstrate precise and independent control of the size, shape and chemical compositions of fabricated particles and result in uniform particles. Also, these processes are applicable to biocompatible polymers such as PEG derivatives. Finally, they provide an efficient strategy to incorporate therapeutic drugs as well as imaging agents in the polymer matrix through the premixing process. Nevertheless, there are still many challenges that need to be addressed. For example, the yield or throughput of these top-down methods is still far below the bottom-up methods. Ingenious engineering solutions are greatly needed to build high throughput equipment and establish the scale-up infrastructure necessary for mass production of shape-specific particles.

Pharmacological and biological functions of shape-specific particulates

The rapid development of new techniques to fabricate nanoparticles with specific shapes has opened up exciting opportunities for *in vitro* and *in vivo* applications. One example that highlights the importance of shape on particle's *in vivo* behavior was demonstrated by Geng *et al.*[24] Filamentous diblock copolymer micelles with a 22–60 nm diameter and 2–18 μm length exhibited an extraordinarily prolonged half-life in blood circulation: up to almost a week (Table 2), which is much longer than the half-life (a few hours) for spherical micelles. With longer cylinders, filomicelles loaded with paclitaxel led to improved antitumor activity. The improved targeting efficiency for longer cylinders was thought to be a result of decreased phagocytosis. These results stimulated interest in employing filamentous (long worm-shaped) carriers in nanomedicine. In another *in vivo* study, Muro *et al.*[25] compared the blood clearance rate and targeted accumulation in tissues of polystyrene spheres (diameter ranges from 0.1 to 10 μm) and elliptical discs (0.1 × 1 × 3 μm) as shown in Table 2. Elliptical discs remained in the circulation for a longer period than all spherical counterparts. Furthermore, the targeted accumulation of discs was significantly higher than for all sphere sizes, even for spheres with a smaller diameter of 100 nm. This *in vivo* evidence clearly demonstrates that shape affects endothelial targeting efficiency. Gratton *et al.*[63] reported preliminary biofunctional studies on the *in vivo* behavior of PRINT® particles. Pharmacokinetic and organ distribution studies were conducted (Table 2), although no spherical counterpart was directly compared with the PRINT® PEG rod-shaped particles during these *in vivo* studies.

An *in vitro* study on the cellular localization of discal and spherical particles by endothelial cells was performed by Muro *et al.*[25] Remarkable reduction of internalization was observed for discs relative to spheres despite the two particles sharing the same endocytic pathway. Champion and Mitragotri [65] reported the importance of shape on phagocytosis, which is a pathway for cellular internalization of micron scale particles. Local shape at the contact point between particle and cell was the dominant parameter that initiated phagocytosis. For example, worm-shaped polystyrene particles (Figure 2b1) showed reduced phagocytosis compared with the spherical ones of the same volume.[66] A similar observation was also reported for filomicelles, and increase of the aspect-ratio of filomicelles leads to reduced phagocytosis by human macrophage cells. The decreased clearance by phagocytosis could contribute to the elongated lifetime of long filomiceles in blood circulation.

Gratton *et al.*[61] performed an *in vitro* study on cellular internalization of acrylic rod-shaped particles into HeLa

Table 2 Reported *in vivo* studies on shape-specific polymeric particles

Fabrication techniques	Filomicelles[24]	Stretching of spherical particles[25]	PRINT®[63]
Shape and size	Worms: Φ22–60 nm $L = 2$–18 μm	Elliptical discs: 100 nm × 1 μm × 3 μm (0.24 μm^3)	Rods: Φ200 × 150 nm (2×10^{-2} μm^3)
Matrix material	PEG-poly(ethylene), PEG-poly(ε-caprolactone)	Polystyrene	78 % (w/w) PEGDA (Mw = 1k), 20% (w/w) PEGMA and 1% (w/w) *para*-hydroxystyrene
Functional agents or labeling	Hydrophobic fluorescent dye, paclitaxel	Anti-ICAM or immunoglobulin G coating, [$Na^{125}I$] labeling	[$Na^{125}I$] labeling, specific activity 4.3 μCi/mg
Concentration of particle suspension	5 mg/mL in PBS	N/A	10 mg/mL in H_2O
Injection dose	0.5 mL in rats, or 0.1 mL in C57 mice	~10 mg/kg in mice[64]	~20 mg/kg in mice 0.32 mg [^{125}I] particles
Pharmacokinetics	Lifespan in blood circulation: 2 μm: 1 d; 4 μm: 2 d; 8 μm: 4 d; ≥18 μm: 6 d	N/A	Apparent distribution $t_{1/2} = 17$ min (followed by redistribution with a $t_{1/2}$ = of 3.3 h)
Organ distribution	4 d after injection: major in liver and spleen, measurable in kidneys, moderate in lungs	30 min after injection: lower uptake in liver but targeted to the lung	24 h after injection: 30% in liver and spleen, 1% in kidneys, heart and lungs

PRINT, particle replication in non-wetting template; PEGA, polyethylene glycol; PEGDA, polyethylene glycol diacrylatel; PEGMA, polyethylene glycol methacrylate; ICAM, intercellular adhesion molecule 1

cells. They observed the preferential uptake of cylindrical particles compared with spherical counterparts of the same volume. More interestingly, the dependence on the aspect-ratio (length to diameter, γ) of cylindrical particles was revealed for the cellular internalization. The internalization of high aspect-ratio particles ($\gamma = 3$) was more efficient than low aspect-ratio particles ($\gamma = 1$). As will be depicted in the following section, cellular internalization is a key step for intravascular delivery. This observation revealed that shape could be an important modifiable design parameter that can alter the efficiency of drug delivery.

The degradation mechanism for shape-specific nanoparticles was expected to be significantly different from spherical ones[41] because of differences in the ratio of surface area to volume.[67] However, there is currently no direct supporting evidence for this. Degradation kinetics for polymeric carriers affects the kinetics of drug release as well as the local toxicity. Igarashi[68] and Vega-Villa *et al.*[69] contended that non-spherical polymeric carriers reduced cytotoxicity due to the specific distribution to specific organs, whereas Medina *et al.*[70] argued that intrinsic toxicity could be enhanced due to high reactivity from the large ratio of surface to volume.

In summary, shape alters the biological activity of polymeric carriers in several nanomedicine case studies. A clear elucidation of the precise role of shape requires comprehensive analysis of more systematically designed experiments, and correlation of the shape parameters with *in vivo* functional properties.

Computational modeling: effect of shape on intravascular delivery of particulates

In vivo, nanoparticles are exposed to complex biological and physiological environments that cannot be easily simulated experimentally. Computational models that simulate biological conditions can greatly facilitate the testing and verification of shape-specific hypotheses for biological systems. For intravascular delivery, the efficacy of targeted delivery of nanoparticles is impacted by several fundamental processes:[71–74] margination to the periphery of blood vessels, adhesion to endothelial cells via cell/particle interactions and cellular internalization. Margination and adhesion of particles under vascular flow conditions are within the scope of intravascular dynamics modeling[75–80] while cellular level modeling[78,79,81–86] can be used to study the adhesion forces between particles and targeted cells and follow cellular internalization.

Intravascular dynamics

Djohari and Dormidontova[87] studied the kinetics of spherical nanoparticle targeting to the cell surface using dissipative particle dynamics. The shape of the adsorbed nanoparticle was found to become ellipsoidal with increasing binding energy. Decuzzi *et al.*[76,81,88] proposed several mathematical models to describe the margination and adhesion of particles to the endothelial cell surface in circulation. Unlike spheres, the velocity of margination can be altered by varying the aspect-ratio of non-spherical particles. They also reported that transport and attachment of particles is strongly dependent on particle size and shape in addition to other mechanical or biological properties of particles and targeted cells. When a particle approaches a cell surface (usually within 20 nm), ligands on the particle surface begin to bind to receptors on the cell surface, forming ligand–receptor bonds. The process of ligand–receptor binding is stochastic. The probability of adhesion (Pa) for a particle is defined as the probability of having at least one ligand–receptor bond formed between the particle and cell surface. In their work, the adhesion probability of an oblate-shaped particle is formulated as a function of the surface density of receptors and ligands, contact area for the particle and the dislodging force due to hydrodynamic forces. These studies provided valuable information on spherical and oblate particles, where oblate particles showed more effective adhesion than spheres. However, in these studies, margination and adhesion processes were modeled separately when in reality they are interactive. Also, only oblate-shaped nanoparticles were intensively modeled, leaving other shapes unexplored.

Liu *et al.*[78,79,86] developed numerical methods based on immersed finite element and molecular dynamics for the simulation of biological systems at the nanoscale. These methods were used in several applications at the bio–nano interface, including modeling of 3D aggregation and deformation of red blood cells in capillaries, deposition of platelets on injured vessel walls, and the capture of viruses by biosurfaces. Applying this model, Liu and coworkers[89] demonstrated the influence of shape and aspect-ratio on the dynamics and probability of adhesion under flow conditions. Numerical simulation illustrated that tumbling and 'pin-over' effects from non-spherical shapes could help the adhesion. Taking rod-shaped particles as an example (Figure 3a), during tumbling the particle first contacts the wall at the end of long axis with low curvature. Due to shear flow, the non-spherical particle rolls over and aligns itself parallel to the interface, exposing a large area for more receptor–ligand interactions, which leads to firm adhesion. Tumbling of oblate-shaped microparticles such as platelets near a wall surface has been reported in a few studies.[90–92] In contrast, the spherical particle has a limited surface contact and a constant hydrodynamic cross-section, which makes it easy to detach from the surface. Based on this model and the model by Decuzzi and Ferrari,[81] the adhesion probability of rods, discs and spheres to the blood vessel walls (Figure 3b) was plotted as a function of volume. Particle volume of 200 nm in at least one dimension representing the spleen filtration threshold is indicated as lines in Figure 3b. Particles with volumes below the spleen filtration limit are of interest for nanomedicine applications. When the volume of spheres increases, the adhesion probability increases initially due to the increasing number of receptors available for adhesion, but then decreases due to the larger relative shear force experienced by larger spherical particles. This increase in shear with size is due to the increased cross-sectional area of the particles that can encounter the higher flow rates

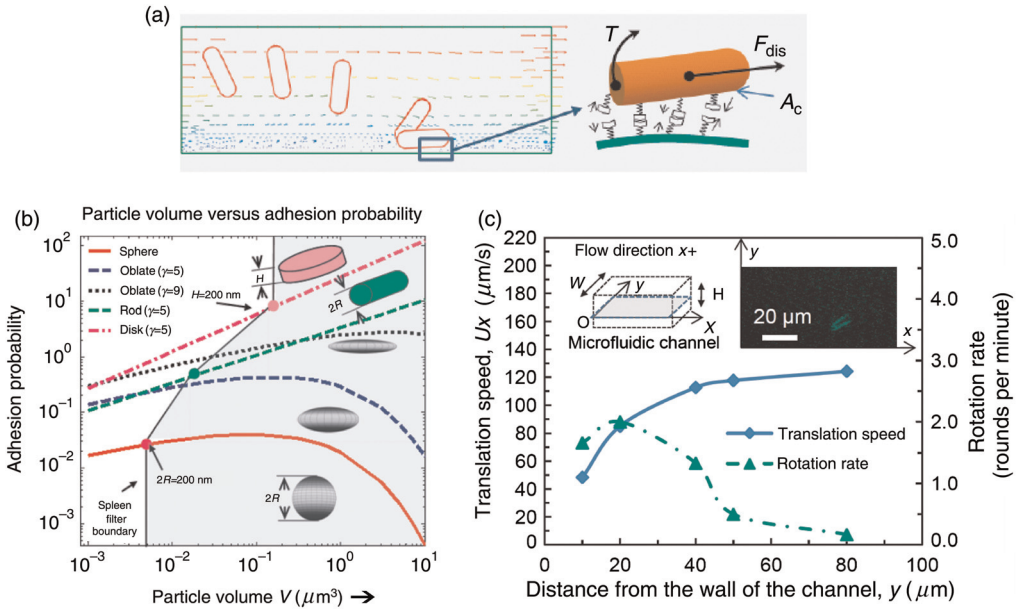

Figure 3 Dynamic particle adhesion model. (a) Simulation of dynamic adhesion process: margination, tumbling, pin-over and firm adhesion. Inset shows ligand–receptor-binding dynamics, where A_c is the contact area of particle to the cell surface, F_{dis} is the dislodging force comprised of two components, drag force along the flow direction and torque T due to tumbling. (b) Adhesion probability as a function of the volume of nanoparticles with various shapes. γ denotes the aspect-ratio. (c) Translation speed and rotation rate of worm-shaped particles ($\Phi \sim 80$ nm and $L \sim 10$ μm) as a function of the position inside the microfluidic channel ($W = 200$ μm and $H = 150$ μm) under 100 μm/s nominal flow as shown in inset. The microfluidic channel was made from polydimethylsiloxane directing to coverslip and the flow is controlled by a Harvard® syringe pump system (A color version of this figure is available in the online journal)

toward the center of blood vessels. For disc- and rod-shaped particles, this occurs at much larger volumes (out of the plot range). These analytical results indicated that rods and discs have higher adhesion probability over spheres because of tumbling and larger contact areas.

Experimental evidence was observed to support these computational modeling results. A preliminary microfluidic flow test on worm-shaped ($\Phi \sim 80$ nm and $L \sim 10$ μm) nanoparticles is shown in Figure 3c. The translation speed of these nano-worms decreases as they are close to the wall, which satisfies the laminar flow in a rectangular channel. The rotation rate, on the other hand, increases when nano-worms are close to the wall of the channel due to the increased shear rate. The tumbling of nano-worm particles will in turn increase the adhesion probability to the wall surface with increased surface contact (Figure 3a and b) as predicted by the modeling. This result is in agreement with a recent report on rod-shaped particles exhibiting significantly higher adhesion than spheres under microfluidic flow conditions by Doshi *et al.*[93]

Cellular uptake

Cellular uptake involves initial firm adhesion and subsequent cellular internalization. Firm adhesion, which counteracts the forces that can dislodge the particle during the initiation of endocytosis, is important for intravascular targeting applications.[74] The adhesive force depends on the strength of ligand–receptor interactions[84,85] as well as non-specific interactions.[82] Champion *et al.*[41] and Mitragotri and co-workers[93] stated that the shape of the particle, especially the profile extending away from the contact interface into the flow, will affect the longevity of specific adhesion. This is in accordance with the modeling by Decuzzi *et al.* who reported dependence on aspect-ratio for the adhesive strength.

For cellular internalization, well-documented studies based on spherical particles[94–97] indicate that receptor-mediated endocytosis is the most efficient pathway for internalization of nanoparticles,[94,97] while micron-sized particles are usually internalized via phagocytosis.[59,83] However, this rule needs re-evaluation for non-spherical particles since they have different sizes along different dimensions. The internalization properties are dependent on the physical and surface properties of the particles, including the particle shape, size, surface charge, hydrophobicity and ligand–receptor binding affinity. Recently developed theoretical modeling by Decuzzi and Ferrari[83] predicted that the internalization of cylindrical particles depends on their aspect-ratio (γ) and volume. Particles with low γ were expected to be more easily internalized than particles with high γ. They observed that elongated particles in contact with their major axis (long dimension) parallel to the interface are less prone to internalization than particles normal to the interface. Similar conclusions at the micron scale were drawn by Champion and Mitragotri[65] in their modeling of phagocytosis. They plotted the internalization velocity versus a characteristic angle Ω, which varies between 0° and 90°. The rate of internalization of non-spherical particles at $\Omega = 90°$ (major axis perpendicular to the interface) was much higher than that at $\Omega = 0°$ (major axis parallel to the interface). These data clearly illustrated the effect that shape, curvature (at local contact with cell) and aspect-ratio can have over the internalization of particles. It is still unclear whether shape

will affect other fundamental steps in drug delivery such as intracellular trafficking and extravesicular transportation after the internalization.[41] Although still far from perfect, insights from computational modeling can stimulate ideas for experimental studies to investigate shape-dependent effects on the biological behavior of nanoparticulate platforms.

Conclusions

Recent discoveries of the unique shape effects on biological functions at nanoscale have spawned multiple shape-specific particulate platforms for nanomedicine applications. Various techniques for the fabrication of non-spherical particles have been established. Many of these techniques, such as PRINT®, stretching spherical particles, S-FIL and TIP, hold great promise because of their ability to simultaneously and independently control shape, size and chemical compositions of fabricated polymeric nanoparticles. Computational models of the effects of particle shape on intravascular dynamics and cellular uptake have been developed. Both modeling data and experimental results indicate that for particulate platforms, shape can have a profound impact on pharmacokinetics and pharmacodynamics.

Future advances in the implementation of shape-specific nanomedicine would include the capability to scale-up without sacrificing the precise control over size and shape. The development of efficient methods for harvesting imprinted nanoparticles is also important for template-based techniques. Also necessary is a well-controlled, systematic study of the effects of shape on particle behavior under biologically relevant conditions. Computational models also need to be integrated to elucidate the effects of shape on the degradation profile, intra- and extracellular trafficking of particles. Only with the mechanistic understanding on how shape would affect fundamental processes during *in vivo* targeting applications, can a rational design incorporating shape into a given nanoparticulate platform be possible.

Author contributions: All authors contributed to the writing and proofreading of the manuscript.

ACKNOWLEDGEMENTS

This work is supported by the Department of the Army (W81XWH-BAA08) and Montcrief Foundation (WH and JG), the National Science Foundation (CBET-0955214) and National Institutes of Health (EB009786) (YL), and American Academy of Otolaryngology-Head and Neck Surgery Foundation (AAO-HNSF) through the Percy Memorial Research Award to BDS. GH is supported by a Susan G Komen foundation postdoctoral fellowship (PDF0707216).

REFERENCES

1 Emerich DF. Nanomedicine – prospective therapeutic and diagnostic applications. *Expert Opin Biol Ther* 2005;**5**:1–5
2 Freitas RA Jr. What is nanomedicine? *Nanomedicine* 2005;**1**:2–9
3 Moghimi SM, Hunter AC, Murray JC. Nanomedicine: current status and future prospects. *FASEB J* 2005;**19**:311–30
4 Blanco E, Kessinger CW, Sumer BD, Gao J. Multifunctional micellar nanomedicine for cancer therapy. *Exp Biol Med (Maywood)* 2009;**234**:123–31
5 Ferrari M. Cancer nanotechnology: opportunities and challenges. *Nat Rev Cancer* 2005;**5**:161–71
6 Freitas RA Jr. The future of nanofabrication and molecular scale devices in nanomedicine. *Stud Health Technol Inform* 2002;**80**:45–59
7 Hughes GA. Nanostructure-mediated drug delivery. *Nanomedicine* 2005;**1**:22–30
8 Langer R. Drug delivery and targeting. *Nature* 1998;**392**:5–10
9 Peer D, Karp JM, Hong S, Farokhzad OC, Margalit R, Langer R. Nanocarriers as an emerging platform for cancer therapy. *Nat Nanotechnol* 2007;**2**:751–60
10 Sanvicens N, Marco MP. Multifunctional nanoparticles–properties and prospects for their use in human medicine. *Trends Biotechnol* 2008;**26**:425–33
11 Sukhorukov GB, Mohwald H. Multifunctional cargo systems for biotechnology. *Trends Biotechnol* 2007;**25**:93–8
12 Sumer B, Gao J. Theranostic nanomedicine for cancer. *Nanomedicine (Lond)* 2008;**3**:137–40
13 Samad A, Sultana Y, Aqil M. Liposomal drug delivery systems: an update review. *Curr Drug Deliv* 2007;**4**:297–305
14 Sharma G, Anabousi S, Ehrhardt C, Ravi Kumar MN. Liposomes as targeted drug delivery systems in the treatment of breast cancer. *J Drug Target* 2006;**14**:301–10
15 Sutton D, Nasongkla N, Blanco E, Gao J. Functionalized micellar systems for cancer targeted drug delivery. *Pharm Res* 2007;**24**:1029–46
16 Torchilin VP. Targeted polymeric micelles for delivery of poorly soluble drugs. *Cell Mol Life Sci* 2004;**61**:2549–59
17 Gao X, Yang L, Petros JA, Marshall FF, Simons JW, Nie S. *In vivo* molecular and cellular imaging with quantum dots. *Curr Opin Biotechnol* 2005;**16**:63–72
18 Smith AM, Ruan G, Rhyner MN, Nie S. Engineering luminescent quantum dots for *in vivo* molecular and cellular imaging. *Ann Biomed Eng* 2006;**34**:3–14
19 Koenig S, Chechik V. Shell cross-linked Au nanoparticles. *Langmuir* 2006;**22**:5168–73
20 Lou X, Wang C, He L. Core-shell Au nanoparticle formation with DNA–polymer hybrid coatings using aqueous ATRP. *Biomacromolecules* 2007;**8**:1385–90
21 Duncan R, Izzo L. Dendrimer biocompatibility and toxicity. *Adv Drug Deliv Rev* 2005;**57**:2215–37
22 Najlah M, D'Emanuele A. Crossing cellular barriers using dendrimer nanotechnologies. *Curr Opin Pharmacol* 2006;**6**:522–7
23 Mitragotri S, Lahann J. Physical approaches to biomaterial design. *Nat Mater* 2009;**8**:15–23
24 Geng Y, Dalhaimer P, Cai S, Tsai R, Tewari M, Minko T, Discher DE. Shape effects of filaments versus spherical particles in flow and drug delivery. *Nat Nanotechnol* 2007;**2**:249–55
25 Muro S, Garnacho C, Champion JA, Leferovich J, Gajewski C, Schuchman EH, Mitragotri S, Muzykantov VR. Control of endothelial targeting and intracellular delivery of therapeutic enzymes by modulating the size and shape of ICAM-1-targeted carriers. *Mol Ther* 2008;**16**:1450–8
26 Liu Z, Cai W, He L, Nakayama N, Chen K, Sun X, Chen X, Dai H. *In vivo* biodistribution and highly efficient tumour targeting of carbon nanotubes in mice. *Nat Nanotechnol* 2007;**2**:47–52
27 Park J-H, Maltzahn Gv, Zhang L, Schwartz MP, Ruoslahti E, Bhatia SN, Sailor MJ. Magnetic iron oxide nanoworms for tumor targeting and imaging. *Adv Mater* 2008;**20**:1630–5
28 Park JH, von Maltzahn G, Zhang L, Derfus AM, Simberg D, Harris TJ, Ruoslahti E, Bhatia SN, Sailor MJ. Systematic surface engineering of magnetic nanoworms for *in vivo* tumor targeting. *Small* 2009;**5**:694–700
29 Gref R, Minamitake Y, Peracchia MT, Trubetskoy V, Torchilin V, Langer R. Biodegradable long-circulating polymeric nanospheres. *Science* 1994;**263**:1600–3
30 Guha S, Mandal BM. Dispersion polymerization of acrylamide. III. Partial isopropyl ester of poly(vinyl methyl ether-alt-maleic anhydride) as a stabilizer. *J Colloid Interface Sci* 2004;**271**:55–9
31 Heurtault B, Saulnier P, Pech B, Proust JE, Benoit JP. Physico-chemical stability of colloidal lipid particles. *Biomaterials* 2003;**24**:4283–300

32 Dendukuri D, Gu SS, Pregibon DC, Hatton TA, Doyle PS. Stop-flow lithography in a microfluidic device. *Lab Chip* 2007;**7**:818–28
33 Dendukuri D, Tsoi K, Hatton TA, Doyle PS. Controlled synthesis of nonspherical microparticles using microfluidics. *Langmuir* 2005;**21**:2113–16
34 Gratton SE, Napier ME, Ropp PA, Tian S, DeSimone JM. Microfabricated particles for engineered drug therapies: elucidation into the mechanisms of cellular internalization of PRINT particles. *Pharm Res* 2008;**25**:2845–52
35 Herlihy KP, DeSimone JM. Magneto-polymer composite particles fabricated utilizing patterned perfluoropolyether elastomer molds. In: Lercel MJ, ed. *Emerging Lithographic Technologies XI*; 2007; San Jose, CA, USA: SPIE
36 Kelly JY, DeSimone JM. Shape-specific, monodisperse nano-molding of protein particles. *J Am Chem Soc* 2008;**130**:5438–9
37 Petros RA, Ropp PA, DeSimone JM. Reductively labile PRINT particles for the delivery of doxorubicin to HeLa cells. *J Am Chem Soc* 2008;**130**:5008–9
38 Rolland JP, Maynor BW, Euliss LE, Exner AE, Denison GM, DeSimone JM. Direct fabrication and harvesting of monodisperse, shape-specific nanobiomaterials. *J Am Chem Soc* 2005;**127**:10096–100
39 Zhang H, Nunes JK, Gratton SEA, Herlihy KP, Pohlhaus PD, DeSimone JM. Fabrication of multiphasic and regio-specifically functionalized PRINT(R) particles of controlled size and shape. *New J Phys* 2009;**11**:075018
40 Champion JA, Katare YK, Mitragotri S. Making polymeric micro- and nanoparticles of complex shapes. *Proc Natl Acad Sci USA* 2007;**104**:11901–4
41 Champion JA, Katare YK, Mitragotri S. Particle shape: a new design parameter for micro- and nanoscale drug delivery carriers. *J Control Release* 2007;**121**:3–9
42 Ho CC, Keller A, Odell JA, Ottewill RH. Preparation of monodisperse ellipsoidal polystyrene particles. *Colloid Polym Sci* 1993;**271**:469–79
43 Glangchai LC, Caldorera-Moore M, Shi L, Roy K. Nanoimprint lithography based fabrication of shape-specific, enzymatically-triggered smart nanoparticles. *J Control Release* 2008;**125**:263–72
44 Buyukserin F, Aryal M, Gao J, Hu W. Fabrication of polymeric nanorods using bilayer nanoimprint lithography. *Small* 2009;**5**:1632–6
45 Tao L, Crouch A, Yoon F, Lee BK, Guthi JS, Kim J, Gao J, Hu W. Surface energy induced patterning of organic and inorganic materials on heterogeneous Si surfaces. *J Vac Sci Technol B* 2007;**25**:1993–7
46 Tao L, Zhao XM, Gao JM, Hu W. Lithographically defined uniform worm-shaped polymeric nanoparticles. *Nanotechnology* 2010;**21**:095301
47 Yang Z, Huck WT, Clarke SM, Tajbakhsh AR, Terentjev EM. Shape-memory nanoparticles from inherently non-spherical polymer colloids. *Nat Mater* 2005;**4**:486–90
48 Chou SY, Krauss PR, Renstrom PJ. Nanoimprint lithography. *J Vacuum Sci Technol B* 1996;**14**:4129–33
49 Colburn M, Johnson SC, Stewart MD, Damle S, Bailey TC, Choi B, Wedlake M, Michaelson TB, Sreenivasan SV, Ekerdt JG, Willson CG. Step and flash imprint lithography: a new approach to high-resolution patterning. *Proc SPIE* 1999;**3676**:379–89
50 Xia Y, Whitesides GM. Soft lithography. *Angew Chem Int Ed Engl* 1998;**37**:550–75
51 Piner RD, Zhu J, Xu F, Hong S, Mirkin CA. 'Dip-Pen' nanolithography. *Science* 1999;**283**:661–3
52 Bruinink CM, Péter M, Maury PA, de Boer M, Kuipers L, Huskens J, Reinhoudt DN. Capillary force lithography: fabrication of functional polymer templates as versatile tools for nanolithography. *Adv Funct Mater* 2006;**16**:1555–65
53 Jackman RJ, Wilbur JL, Whitesides GM. Fabrication of submicrometer features on curved substrates by microcontact printing. *Science* 1995;**269**:664–6
54 Zaumseil J, Meitl MA, Hsu JWP, Acharya BR, Baldwin KW, Loo Y-L, Rogers JA. Three-dimensional and multilayer nanostructures formed by nanotransfer printing. *Nano Lett* 2003;**3**:1223–7
55 Doshi N, Zahr AS, Bhaskar S, Lahann J, Mitragotri S. Red blood cell-mimicking synthetic biomaterial particles. *Proc Natl Acad Sci USA* 2009;**106**:21495–9
56 Rolland JP, Hagberg EC, Denison GM, Carter KR, De Simone JM. High-resolution soft lithography: enabling materials for nanotechnologies. *Angew Chem Int Ed Engl* 2004;**43**:5796–9
57 Lee H-J, Ro HW, Soles CL, Jones RL, Lin EK, Wu W-l, Hines DR. Effect of initial resist thickness on residual layer thickness of nanoimprinted structures. *J Vac Sci Technol B* 2005;**23**:3023–7
58 Scheer HC, Schulz H, Hoffmann T, Torres CMS. Problems of the nanoimprinting technique for nanometer scale pattern definition. *J Vac Sci Technol B* 1998;**16**:3917–21
59 Canelas DA, Herlihy KP, DeSimone JM. Top-down particle fabrication: control of size and shape for diagnostic imaging and drug delivery. *Wiley Interdiscip Rev Nanomed Nanobiotechnol* 2009;**1**:391–404
60 Truong TT, Lin R, Jeon S, Lee HH, Maria J, Gaur A, Hua F, Meinel I, Rogers JA. Soft lithography using acryloxy perfluoropolyether composite stamps. *Langmuir* 2007;**23**:2898–905
61 Gratton SE, Ropp PA, Pohlhaus PD, Luft JC, Madden VJ, Napier ME, DeSimone JM. The effect of particle design on cellular internalization pathways. *Proc Natl Acad Sci USA* 2008;**105**:11613–18
62 Euliss LE, DuPont JA, Gratton S, DeSimone J. Imparting size, shape, and composition control of materials for nanomedicine. *Chem Soc Rev* 2006;**35**:1095–104
63 Gratton SE, Pohlhaus PD, Lee J, Guo J, Cho MJ, Desimone JM. Nanofabricated particles for engineered drug therapies: a preliminary biodistribution study of PRINT nanoparticles. *J Control Release* 2007;**121**:10–18
64 Muro S, Dziubla T, Qiu W, Leferovich J, Cui X, Berk E, Muzykantov VR. Endothelial targeting of high-affinity multivalent polymer nanocarriers directed to intercellular adhesion molecule 1. *J Pharmacol Exp Ther* 2006;**317**:1161–9
65 Champion JA, Mitragotri S. Role of target geometry in phagocytosis. *Proc Natl Acad Sci USA* 2006;**103**:4930–4
66 Champion JA, Mitragotri S. Shape induced inhibition of phagocytosis of polymer particles. *Pharm Res* 2009;**26**:244–9
67 Hsieh DS, Rhine WD, Langer R. Zero-order controlled-release polymer matrices for micro- and macromolecules. *J Pharm Sci* 1983;**72**:17–22
68 Igarashi E. Factors affecting toxicity and efficacy of polymeric nanomedicines. *Toxicol Appl Pharmacol* 2008;**229**:121–34
69 Vega-Villa KR, Takemoto JK, Yanez JA, Remsberg CM, Forrest ML, Davies NM. Clinical toxicities of nanocarrier systems. *Adv Drug Deliv Rev* 2008;**60**:929–38
70 Medina C, Santos-Martinez MJ, Radomski A, Corrigan OI, Radomski MW. Nanoparticles: pharmacological and toxicological significance. *Br J Pharmacol* 2007;**150**:552–8
71 Decuzzi P, Pasqualini R, Arap W, Ferrari M. Intravascular delivery of particulate systems: does geometry really matter? *Pharm Res* 2009;**26**:235–43
72 Jain RK. Delivery of molecular and cellular medicine to solid tumors. *Adv Drug Deliv Rev* 2001;**46**:149–68
73 Moghimi SM, Hunter AC, Murray JC. Long-circulating and target-specific nanoparticles: theory to practice. *Pharmacol Rev* 2001;**53**:283–318
74 Neri D, Bicknell R. Tumour vascular targeting. *Nat Rev Cancer* 2005;**5**:436–46
75 Decuzzi P, Causa F, Ferrari M, Netti PA. The effective dispersion of nanovectors within the tumor microvasculature. *Ann Biomed Eng* 2006;**34**:633–41
76 Decuzzi P, Lee S, Bhushan B, Ferrari M. A theoretical model for the margination of particles within blood vessels. *Ann Biomed Eng* 2005;**33**:179–90
77 Gentile F, Chiappini C, Fine D, Bhavane RC, Peluccio MS, Cheng MM, Liu X, Ferrari M, Decuzzi P. The effect of shape on the margination dynamics of non-neutrally buoyant particles in two-dimensional shear flows. *J Biomech* 2008;**41**:2312–18
78 Liu WK, Liu Y, Farrell D, Zhang L, Wang XS, Fukui Y, Patankar N, Zhang Y, Bajaj C, Lee J, Hong J, Chen X, Hsu H. Immersed finite element method and its applications to biological systems. *Comput Methods Appl Mech Eng* 2006;**195**:1722–49
79 Liu Y, Liu WK. Rheology of red blood cell aggregation by computer simulation. *J Comp Phys* 2006;**220**:139–54
80 Liu Y, Zhang L, Wang X, Liu WK. Coupling of Navier–Stokes equations with protein molecular dynamics and its application to hemodynamics. *Int J Numer Meth Fluids* 2004;**46**:1237–52
81 Decuzzi P, Ferrari M. The adhesive strength of non-spherical particles mediated by specific interactions. *Biomaterials* 2006;**27**:5307–14

82 Decuzzi P, Ferrari M. The role of specific and non-specific interactions in receptor-mediated endocytosis of nanoparticles. *Biomaterials* 2007;**28**:2915–22
83 Decuzzi P, Ferrari M. The receptor-mediated endocytosis of nonspherical particles. *Biophys J* 2008;**94**:3790–7
84 Gao H, Shi W, Freund LB. Mechanics of receptor-mediated endocytosis. *Proc Natl Acad Sci USA* 2005;**102**:9469–74
85 Freund LB, Lin Y. The role of binder mobility in spontaneous adhesive contact and implications for cell adhesion. *J Mech Phys Solids* 2004;**52**:2455–72
86 Liu Y, Liu WK, Belytschko T, Patankar N, To AC, Kopacz A, Chung J-H. Immersed electrokinetic finite element method. *Int J Numer Meth Eng* 2007;**71**:379–405
87 Djohari H, Dormidontova EE. Kinetics of nanoparticle targeting by dissipative particle dynamics simulations. *Biomacromolecules* 2009;**10**:3089–97
88 Decuzzi P, Lee S, Decuzzi M, Ferrari M. Adhesion of microfabricated particles on vascular endothelium: a parametric analysis. *Ann Biomed Eng* 2004;**32**:793–802
89 Shah S, Liu Y, Hu W, Gao J. Modeling particle shape-dependent dynamics in nanomedicine. *J Nanosci Nanotechnol* 2010 (In press)
90 Gavze E, Shapiro M. Particles in a shear flow near a solid wall: effect of nonsphericity on forces and velocities. *Int J Multiphase Flow* 1997;**23**:155–82
91 Mody NA, King MR. Three-dimensional simulations of a platelet-shaped spheroid near a wall in shear flow. *Phys Fluids* 2005;**17**:113302–12
92 Pozrikidis C. Flipping of an adherent blood platelet over a substrate. *J Fluid Mech* 2006;**568**:161–72
93 Doshi N, Prabhakarpandian B, Rea-Ramsey A, Pant K, Sundaram S, Mitragotri S. Flow and adhesion of drug carriers in blood vessels depend on their shape: a study using model synthetic microvascular networks. *J Control Release* 2010;**146**:196–200
94 Conner SD, Schmid SL. Regulated portals of entry into the cell. *Nature* 2003;**422**:37–44
95 Mukherjee S, Ghosh RN, Maxfield FR. Endocytosis. *Physiol Rev* 1997;**77**:759–803
96 Rejman J, Oberle V, Zuhorn IS, Hoekstra D. Size-dependent internalization of particles via the pathways of clathrin- and caveolae-mediated endocytosis. *Biochem J* 2004;**377**:159–69
97 Smith AE, Helenius A. How viruses enter animal cells. *Science* 2004;**304**:237–42